Heating and flow computations of an amorphous polymer in the liquefier of a material extrusion 3D printer

Franck Pigeonneau, D. Xu, M. Vincent, J.-F. Agassant

Heating and flow computations of an amorphous polymer in the liquefier of a material extrusion 3D printer

F. Pigeonneau*, D. Xu, M. Vincent, J.-F. Agassant

MINES ParisTech, PSL Research University, CEMEF - Centre for material forming, CNRS UMR 7635, CS 10207, rue Claude Daunesse 06904 Sophia Antipolis Cedex, France

Abstract

The heating of a polymer in a liquefier of a material extrusion 3D printer is numerically studied. The problem is investigated by solving the mass, momentum, and energy conservation equations. The polymer is taken as a generalized Newtonian fluid with a dynamical viscosity function of shear rate and temperature. The system of equations is solved using a finite element method. The boundary conditions are adapted by comparison with the previous work of Peng et al. [5] showing that the thermal contact between the polymer and the liquefier is very well established. The limiting printing conditions are studied by determining the length over which the polymer temperature is below the glass transition temperature. This provides a simple relation for the inlet velocity as a function of the working parameters and the polymer properties.

Key words: Polymer; 3D printing; material extrusion; heat transfer; finite element analysis

1. Introduction

One of the most recent manufacturing technologies is additive manufacturing (AM) which emerged in the 1990s [1]. Contrary to the subtractive techniques, the product is built by adding a tiny amount of material step by step. AM offers a new "design freedom" to create products impossible to make with a classical process [2]. Recently, Lee et al. [3] detailed the perspectives of AM in biology. For plastic products, different technologies exist. In powder bed fusion, a laser provides energy to selectively melt a fine granular material. Selective laser melting (SLM) or selective laser sintering (SLS) belong to this kind of process [2]. In material extrusion (ME), an extruder is used to melt the material which is deposited on a substrate [1, 2]. The fused filament fabrication (FFF) belongs to this category.

In material extrusion, three steps are required. A small amount of polymer is melted, added on the ongoing product and finally cooled. This process is presented in detail in the recent review of Goh et al. [4] in which the printing parameters are provided. FFF is

*Corresponding author: Tel. +33 (4) 93 95 74 34, Fax +33 (4) 92 38 97 52.
Email address: franck.pigeonneau@mines-paristech.fr (F. Pigeonneau)

an unsteady and nonisothermal process [5]. The overall thermal behavior of a deposited material has been studied by Costa et al. [6] using a numerical method. The mechanical properties are also studied in this reference.

In the current contribution, investigations will be focused on the fused filament fabrication technology using amorphous polymers melted in an extrusion chamber also called liquefier before the deposition on the build surface. The working parameters of the process are extruder and build surface temperatures, the feeding velocity of polymer filament, the velocity of the print head and the gap between head and substrate.

In FFF, the liquefier is a furnace in which the solid polymer rod is introduced and melted by heat transfer and then forced into a small nozzle. Bellini et al. [7] studied the force required to push the polymer through the extruder by determining the pressure drop. They found the transfer function corresponding to the ratio of the output to the input signals [8, Chap. 20] of the liquefier. More recently, Mackay et al. [9] determined the maximum feed velocity of a FFF 3D printer to have a homogeneous temperature field at the nozzle exit for three polymers. Assuming a plug flow in the liquefier, they investigated the thermal behavior with a dimensionless function representing the temperature. Peng et al. [5] studied experimentally the heating of bisphenol-A polycarbonate using a thermocouple introduced in the polymer rod. They recorded the thermal history of the polymer in the liquefier. By introducing dye markers in the solid polymer rod, the hydrodynamics through the extruder is also investigated. They concluded that the velocity profile is far from the isothermal power-law solution.

To explain the recent contribution of Peng et al. [5], heat and mass transfer are solved numerically inside the extruder. The polymer behaves as a generalized Newtonian fluid. Particular attention will be paid on the thermal resistance between polymer and liquefier. In the present work, two major questions are addressed. What is the temperature history within the hot part of the extruder? How does the inlet velocity impact temperature history?

The problem statement is presented in section 2. Results are detailed and discussed in section 3 with two subsections. The first, § 3.1, is devoted to heating and kinematic behaviors of the polymer. The second, § 3.2, focuses on the traveling distance in the liquefier to reach the glass transition temperature. A short conclusion is given in section 4. Appendix A provides the main properties of two amorphous polymers used to perform the numerical computations.

2. Problem statement

The geometry of the liquefier is taken from the previous work of Peng et al. [5] corresponding to the liquefier of the Cartesio 3D printer, model W09. Figure 1 depicts the interior geometry of the liquefier composed of a cylinder with a diameter close to the polymer rod diameter and a nozzle with a conical geometry that connects the cylinder to a small capillary die. The boundary of the liquefier is composed of the inlet section $\partial\Omega_{\text{in}}$, the surface of the cylinder $\partial\Omega_{\text{cyl}}$, the cone and the capillary die surfaces of the nozzle $\partial\Omega_{\text{noz}}$ and the outlet section $\partial\Omega_{\text{out}}$. The framework has been also represented in Figure 1 with z the axial coordinate and r the radial coordinate. The polymer is introduced from the left side and exits at the other extremity after the convergent.

The fluid motion considered in this work is assumed in steady-state regime. Moreover, the geometry is mainly a uniform conduit apart from the convergent at the end of the

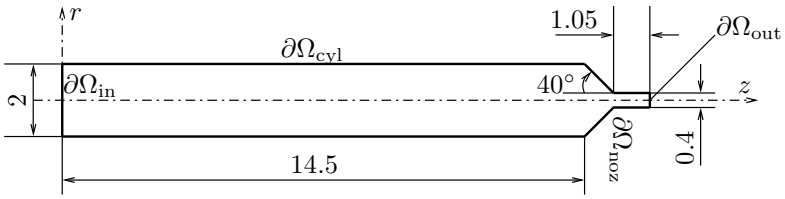

Figure 1: Geometry of the liquefier used for the numerical computations. Dimensions are given in mm.

extruder. As it is very well detailed in the textbook of Bird et al. [10, Chap. 4 & 9], the use of a generalized Newtonian fluid is justified in the fluid domain above T_g. The same behavior is considered below the glass transition temperature. Recently, a similar approach has been used by Xia et al. [11] to study the formation of a filament in FFF. The temperature dependence of the viscosity leads to very high values which mimics a solid behavior. This simplifies the numerical resolution for a multiphase material. The dynamic viscosity is given by the Carreau-Yasuda's law [12, 10] as follows

$$\eta(\dot{\gamma}, T) = \frac{\eta_0 a_T}{\left[1 + (\lambda a_T \dot{\gamma})^a\right]^{(1-n)/a}}, \tag{1}$$

in which η_0 is the Newtonian plateau viscosity, n the power law index, λ a time constant depending on the nature of the polymer and a a parameter to describe the transition between the Newtonian plateau and the power-law regime, T the absolute temperature, $\dot{\gamma}$ the generalized shear rate defined by

$$\dot{\gamma} = \sqrt{2\boldsymbol{D} : \boldsymbol{D}}, \tag{2}$$

and $\boldsymbol{D}$ the rate-of-strain tensor given by

$$\boldsymbol{D} = \frac{1}{2}\left(\boldsymbol{\nabla u} + {}^t\boldsymbol{\nabla u}\right), \tag{3}$$

in which $\boldsymbol{u}$ is the fluid velocity. The symbol ":" in eq. (2) is the double dot product operator defined in [14].

The shift factor a_T follows an Arrhenius's law given by

$$a_T = \exp\left[\frac{E_a}{R}\left(\frac{1}{T} - \frac{1}{T_{\text{ref}}}\right)\right], \tag{4}$$

with E_a the activation energy, R the ideal gas constant and T_{ref} the reference temperature. A Williams-Landel-Ferry (WLF) law [15] would be more suitable for amorphous polymer as it is done in [11]. However, the high value of the activation energy E_a induces a sufficient viscosity increase around T_g to use the Arrhenius's law in the numerical simulations. The shift factors for both polymers are approximately equal to $4 \cdot 10^3$ at T_g and increases exponentially for smaller temperature. In this limit, the fluid moves according to a "solid body motion" with a rate-of-strain tensor equal to zero.

In the following, numerical simulations have been done for two polymers. To compare with the previous results published by Peng et al. [5], the first polymer is a bisphenol-A polycarbonate (Makrolon® 3208). The second polymer is an acrylonitrile butadiene

styrene commonly used in the FFF technology. The parameters of equations (1) and (4) are summarized in Appendix A for both polymers.

The problem is normalized according to Bird et al. [10, Chap. 4]. The spatial coordinates are normalized by the inlet diameter, $D = 2$ mm. The velocity is normalized by the outlet velocity $U = 4Q/(\pi d^2)$ with Q the volumetric flow rate and d the diameter of the nozzle equal to 0.4 mm. The dynamic viscosity is scaled with the viscosity η_0 of the Newtonian plateau. Since the viscosity forces are more important than the inertial forces, the pressure is normalized by $\eta_0 U/D$. The shear rate is also reduced using U/D. Since the range of temperature is between T_0, the inlet temperature, and T_∞ the temperature of the liquefier, the dimensionless temperature is written as follows

$$\theta = \frac{T - T_0}{T_\infty - T_0}. \tag{5}$$

The variation of the specific volume of the polymer as a function of temperature is not taken into account because it is small for amorphous polymers. Consequently, the polymer is assumed incompressible. In the following, the normalized variables are written with an overbar. The balance equations are the following [10]:

$$\boldsymbol{\nabla} \cdot \bar{\boldsymbol{u}} = 0, \tag{6}$$

$$\mathrm{Re}\,\frac{D\bar{\boldsymbol{u}}}{D\bar{t}} = -\boldsymbol{\nabla}\bar{P} + \boldsymbol{\nabla} \cdot \left[2\bar{\eta}(\dot{\bar{\gamma}}, \theta)\bar{\boldsymbol{D}}\right], \tag{7}$$

$$\mathrm{Pe}\,\frac{D\theta}{D\bar{t}} = \boldsymbol{\nabla}^2\theta + \mathrm{Br}\,\bar{\eta}(\dot{\bar{\gamma}}, \theta)\dot{\bar{\gamma}}^2, \tag{8}$$

coming from the volume conservation, the momentum conservation in which the gravity forces are neglected and the energy conservation. In equation (8), the viscous dissipation is taken into account. The three dimensionless numbers, Re the Reynolds number, Pe the Péclet number and Br the Brinkman number [16] are defined by

$$\mathrm{Re} = \frac{\rho U D}{\eta_0}, \tag{9}$$

$$\mathrm{Pe} = \frac{U D}{\kappa}, \tag{10}$$

$$\mathrm{Br} = \frac{\eta_0 U^2}{k(T_\infty - T_0)}, \tag{11}$$

with ρ is the density of the polymer, κ the thermal diffusivity equal to $k/(\rho C_p)$ with k the thermal conductivity and C_p the heat capacity. The thermal properties for both polymers are also provided in appendix A. The dimensionless viscosity is given by

$$\bar{\eta}(\dot{\bar{\gamma}}, \theta) = \frac{a_T}{\left[1 + (\mathrm{Wi}\, a_T \dot{\bar{\gamma}})^a\right]^{(1-n)/a}}, \tag{12}$$

with Wi is a Weissenberg number defined by

$$\mathrm{Wi} = \frac{\lambda U}{D}. \tag{13}$$

Using a maximum extrusion velocity at the outlet of the liquefier equal to 0.5 m/s and the properties of the polycarbonate given in Appendix A, the Reynolds number is

Boundary	Fluid mechanics	Heat transfer
$\partial\Omega_{\text{in}}$	$\bar{\boldsymbol{u}} = \left(\frac{d}{D}\right)^2 \boldsymbol{e}_z$	$\theta = 0$
$\partial\Omega_{\text{cyl}}$	$\bar{\boldsymbol{u}} = 0$	$\frac{\partial\theta}{\partial n} = \text{Nu}(1-\theta)$
$\partial\Omega_{\text{noz}}$	$\bar{\boldsymbol{u}} = 0$	$\theta = 1$
$\partial\Omega_{\text{out}}$	$\bar{\boldsymbol{\sigma}} \cdot \boldsymbol{n} = 0$	-

Table 1: Boundary conditions for fluid mechanics and heat transfer equations in the four boundaries of the liquefier represented in Figure 1.

equal to $2.27 \cdot 10^{-3}$. Consequently, the inertia is negligible in the momentum equation in all situations. The Péclet number is equal to $7.5 \cdot 10^3$. By taking an inlet temperature equal to 24°C and the heating temperature equal to 325°C according to the experimental data of Peng et al. [5], the Brinkman number is equal to 2.2. So, when the extrusion velocity is sufficiently high, the heat transfer by advection and the viscous heating could be important.

Table 1 summarizes the boundary conditions for both the fluid mechanics and heat transfer equations. At the inlet, $\partial\Omega_{\text{in}}$, the normalized velocity is equal to the ratio of the capillary diameter to the cylinder diameter squared. On the cylinder, $\partial\Omega_{\text{cyl}}$, a Fourier (called also Robin) boundary condition has been chosen. The thermal resistance is thus taken into account due to the eventual thin air layer between the extruder and the filament. The Nusselt number, Nu, introduced in Table 1 is defined as follows

$$\text{Nu} = \frac{hD}{k}, \tag{14}$$

with h is the heat transfer coefficient which can be viewed as the inverse of the thermal contact resistance. The Nusselt number is assumed uniform all along the cylinder. As it is difficult to evaluate, the Nusselt number will be determined by comparison between numerical computations and experimental data presented in the next section.

On the convergent and the capillary die surfaces, $\partial\Omega_{\text{noz}}$, a perfect thermal contact is assumed which means that the reduced surface temperature is equal to one. At the outlet, $\partial\Omega_{\text{out}}$, the normal stress corresponding to the natural boundary conditions of the Navier-Stokes equations [17] is imposed equal to zero in which $\bar{\boldsymbol{\sigma}}$ is the dimensionless Cauchy stress tensor equal to $-\bar{P}\boldsymbol{I} + 2\bar{\eta}(\dot{\bar{\gamma}}, \theta)\bar{\boldsymbol{D}}$ with $\boldsymbol{I}$ the identity tensor and $\boldsymbol{n}$ the outward unit normal. This means that the outlet pressure is imposed equal to zero. In real additive manufacturing conditions, the pressure at nozzle exit should be equal to the spreading pressure on the substrate [18]. For the temperature, nothing is applied meaning that θ is unknown right on $\partial\Omega_{\text{out}}$.

A continuous Galerkin finite element method is used to solve the Stokes equations, eqs. (6) and (7) in mixed velocity-pressure formulation using a Taylor-Hood element $P_2 - P_1$ to satisfy the discrete $\inf - \sup$ condition [17]. For the energy equation (8), a discontinuous Galerkin finite element method has been chosen with a polynomial degree equal to P_{2d} to ensure the stabilization of the advection term. For the time integration a backward differentiation formula at the second-order is taken. At each time step, the system is solved sequentially by first solving the Stokes equations and then the energy equation until convergence. Only a 2d-axisymmetric case has been considered. The numerical solver has been written with the Rheolef C++ library developed by Saramito [19].

U_{in} (mm/min)	Pe	Br	Wi
90	562.5	$1.24{\cdot}10^{-2}$	$2.24{\cdot}10^{-2}$
180	1125	$4.94{\cdot}10^{-2}$	$4.47{\cdot}10^{-2}$
270	1687.5	$1.11{\cdot}10^{-1}$	$6.71{\cdot}10^{-2}$

Table 2: Values of the Péclet, Brinkman and Weissenberg numbers for the three inlet velocities.

3. Results and discussion

3.1. Heating and kinematic behaviors of polymer

To control the accuracy of our numerical solver and to set the value of the Nusselt number along the cylinder section of the extruder, computations are done with the working conditions investigated in [5]. In this previous contribution, the authors measured the polycarbonate temperature during its travel in the liquefier by introducing a thermocouple inside the filament. Three values of the polymer velocity at the entrance have been tested. The values of the dimensionless numbers are provided in Table 2 for the three values of the inlet velocity. In the following, even if the three dimensionless numbers change with the inlet velocity, results will be only referenced as a function of the Péclet number.

To adjust the Nusselt number, the thermocouple measurements provided in [5] are exploited. However, the comparison is not so obvious. The experiments are time dependent (the thermocouple is traveling through the liquefier) while the numerical computations are in a steady-state regime. Nevertheless, assuming that the thermocouples have a high temporal resolution, the largest temperature recorded by the thermocouple can be considered as the real temperature at the liquefier exit. Figure 2-(a) plots the temperature as a function of the axial coordinate z for the smallest inlet velocity, i.e. for $\text{Pe} = 562.5$. Four Nusselt numbers are investigated: $\text{Nu} = 1$, 10, 10^2 and ∞. The last one means that the polymer temperature in contact with the wall is set equal to the liquefier temperature. The star corresponds to the maximum of the experimental recording. For the smallest Nusselt number, the polymer temperature at the nozzle exit is below the experimental data. Conversely, for Nusselt numbers larger than or equal to 10, the temperature at the exit obtained numerically is close to the experimental value.

For the second Péclet number, $\text{Pe} = 1125$, the temperature over the axial coordinate is provided in Figure 2-(b) for the four different Nusselt numbers. For the two smallest values of Nu, the exit temperature does not reach the measured value. Conversely, when the Nusselt number is equal to 100 (which corresponds to a nearly perfect contact with the liquefier) the temperature at the exit agrees with the experimental data.

For the largest velocity, i.e. $\text{Pe} = 1687.5$, the temperature over the axial coordinate is depicted in Figure 2-(c). Whatever the Nusselt number, the temperature observed experimentally is never reached. This result is because, for the large Péclet number, the temperature is not radially uniform. Indeed, as it is shown in Figure 3, the temperature exhibits a radial gradient at nozzle exit when the Péclet number is equal to 1125 or 1687.5.

For the smallest Péclet number, the temperature given by the thermocouple is very close to the temperature observed over the radial coordinate since the thermal heterogeneity is limited. For the larger Péclet numbers, the thermocouple integrates a temperature in its neighborhood since the polycarbonate polymer is a semi-transparent media.

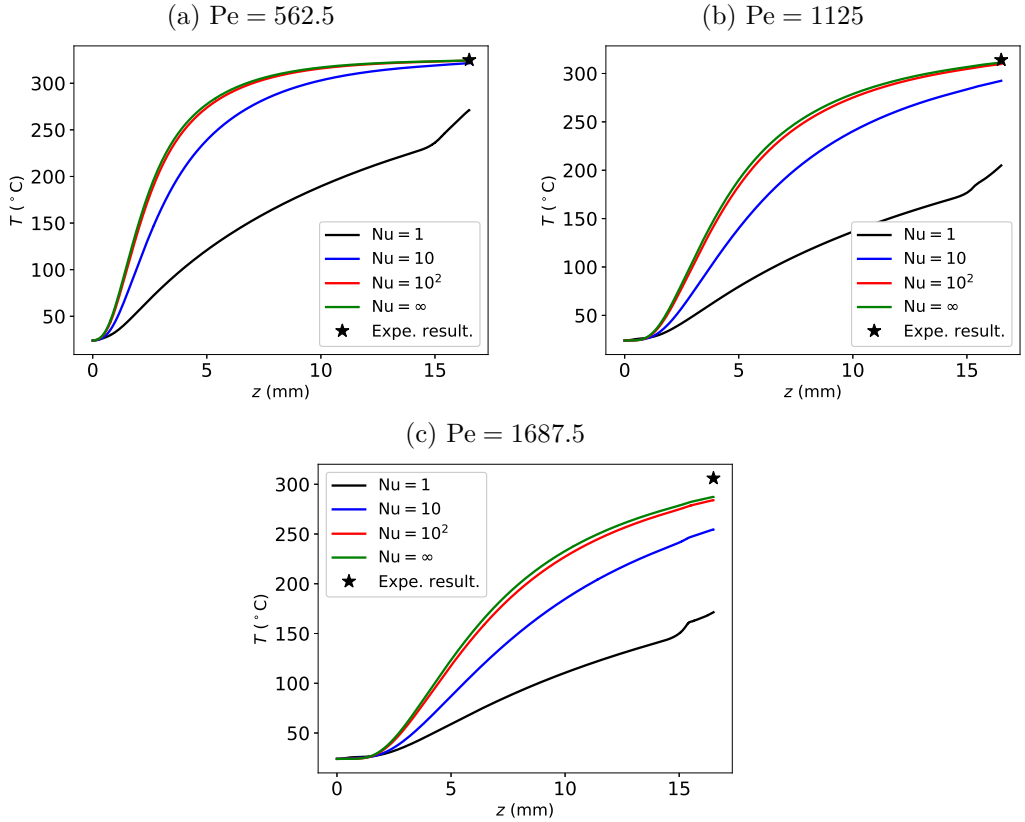

Figure 2: Temperature T (°C) as a function of the axial coordinate z (mm) in $r = 0$ for Nu = 1, 10, 10^2 and ∞ for (a) Pe = 562.5, (b) Pe = 1125 and (c) Pe = 1687.5.

Nevertheless, the temperature recorded by the thermocouple belongs to the range of the temperature obtained numerically.

These results permit us to conclude that the thermal contact between the polymer and the extruder is perfect. Consequently, in the following the temperature of the heating device is applied everywhere along the border of the extruder. These results confirm that the polymer rod heating starts at the entrance of the liquefier. Nevertheless, the two situations investigated experimentally and numerically are not completely equivalent. In the experimental set-up, the melting of a rod is established in a transient regime. Indeed, experiments start with a liquefier without polymer. By introducing the polymer, the liquefier works in an unsteady regime. In the numerical simulation, heating is realized in a steady-state regime which explains the difference between the two situations.

Figure 4 shows the temperature as a function of time for the three extrusion velocities (the z coordinate is replaced by the residence time using the axial velocity). These curves confirm that at small inlet velocity, the temperature of the polymer reaches the heating device temperature. The residence time of the fluid is around five seconds. For Pe = 1125, the residence time is reduced roughly by a factor two. It is noteworthy that for the largest

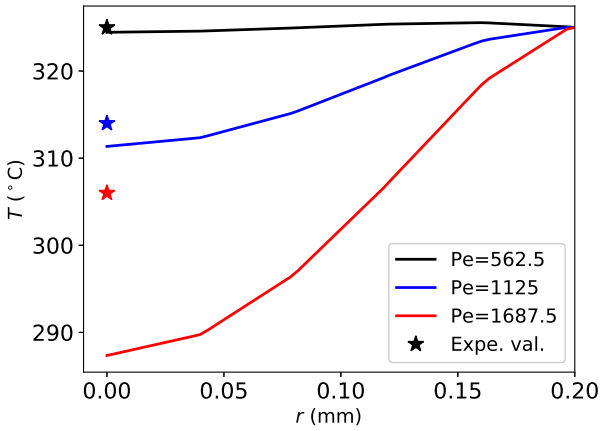

Figure 3: Temperature T (°C) as a function of the radial coordinate r (mm) at the exit of the extruder for Pe = 562.5, 1125 and 1687.5 for a perfect contact on the cylinder section, i.e. Nu = ∞. Stars represent the experimental values found for the three values of the inlet velocity.

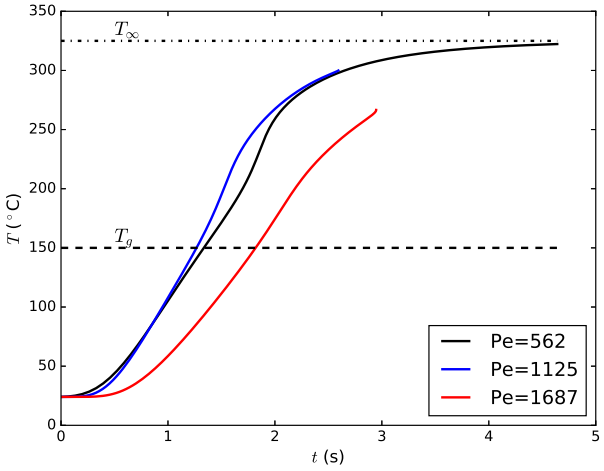

Figure 4: Temperature T (°C) as a function of t (s) right on the axis of the liquefier for Pe = 562.5, 1125 and 1687.5.

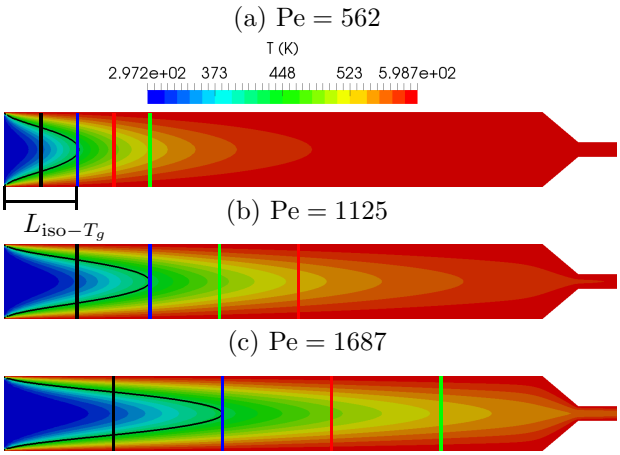

Figure 5: Temperature field (K) for three Péclet numbers. The solid line is the iso-value of $T_g = 423.15$ K. The four vertical lines are the locations of the velocity profiles depicted in Figure 6.

Péclet number the residence time is larger than for Pe = 1125. As observed in Figure 4, for the high Pe value, the temperature in the neighborhood of the inlet stays close to the inlet temperature. Consequently, the velocity profile is closer than a plug flow with a smaller average velocity as it will be shown later.

Numerical results show that the rod is at a temperature above T_g during a shorter range of time when the inlet velocity increases. For Pe = 562.5, 1125 and 1687.5, the times spend above T_g are 3.36, 1.33 and 1.12 s respectively.

Temperature fields are reported in Figure 5 for the three values of the Péclet number. In all investigated situations, the viscous dissipation, the last term of eq. (8), is practically negligible. In the cylinder part, the shear rate is too small to induce viscous dissipation. In the nozzle, the polymer is too hot and so the viscosity too small to develop viscous dissipation. The iso-value corresponding to the glass transition temperature of the bisphenol-A polycarbonate equal to $T_g = 150°$C is reported in black solid line. For the smallest inlet velocity, i.e. Pe = 562.5, the heating of the polymer is efficient since in a large part of the domain the temperature is close to the liquefier temperature. Nevertheless, a cold-core is observed at the inlet where the heat transfer is a competition between advection and thermal diffusion. For this Péclet number, the glass transition temperature is reached on the cylinder axis within 2 mm. The increase of the inlet velocity enlarges the cold-core. The location of the curve $T = T_g$ right on the axis of symmetric which will be designated by $L_{\mathrm{iso}-T_g}$ in the following is equal to 3.94 mm for Pe = 1125 and 5.88 mm for Pe = 1687.5 giving roughly a linear trend of this length with the Péclet number. The distance $L_{\mathrm{iso}-T_g}$ has been reported in Figure 5-(a) for Pe = 562.

To see the coupling between kinematics and heat transfer, the z-component of the velocity $\bar{\boldsymbol{u}}$ is plotted as a function of $\bar{r}$ in Figure 6 at four locations downstream and upstream of the end of the iso-T_g curve for the three Péclet numbers. The first profile in black is in the cold core at one half of $L_{\mathrm{iso}-T_g}$, the second in blue is right on the end of the iso-T_g curve, the third in red is at 1.5 times the $L_{\mathrm{iso}-T_g}$ and the last in green is localized at two times $L_{\mathrm{iso}-T_g}$. The positions of these profiles are reported in Figure 5.

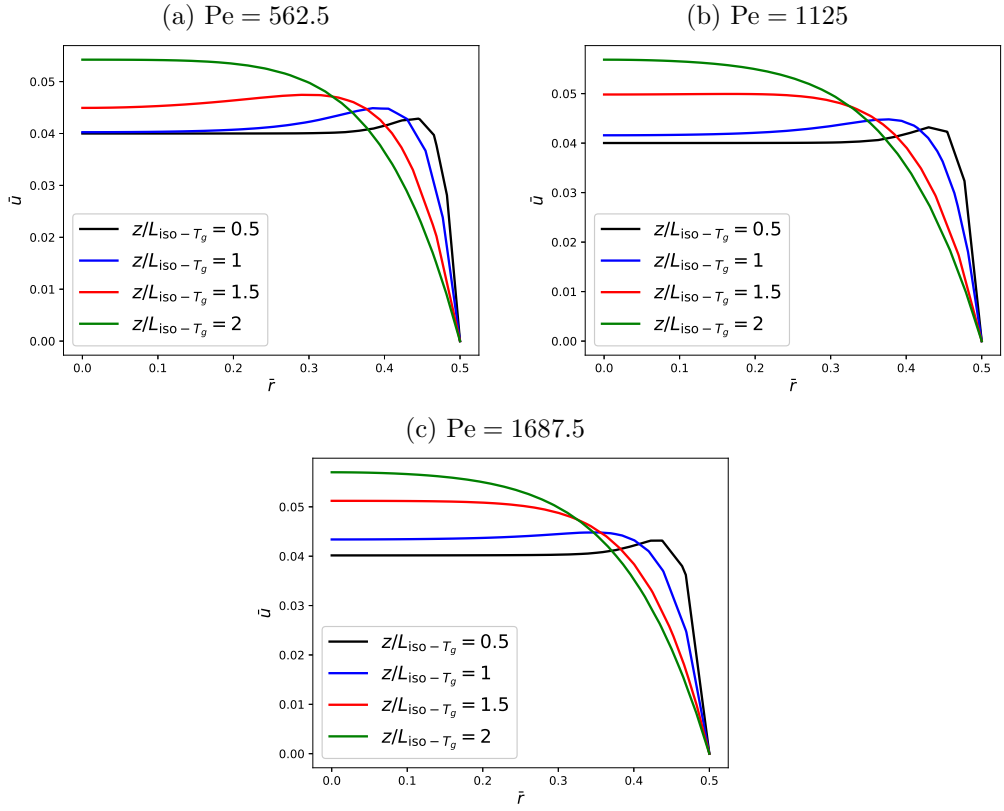

Figure 6: z-component of the velocity $\bar{\boldsymbol{u}}$ as a function of $\bar{r}$ in dimensionless units for (a) Pe = 562.5, (b) Pe = 1125 and (c) Pe = 1687.5.

The velocity profile in the cold core area is characterized by a plug flow. The magnitude is close to the inlet velocity. Whatever the Péclet number, the profiles close to the entrance exhibit an overshoot close to the liquefier wall where the polymer is already melted. The occurrence of a local velocity with a magnitude larger than the inlet velocity can be explained by mass conservation considerations. Since the velocity profiles have been plotted in locations distributed proportionally to the length of the iso T_g-value, the profiles are quite similar for all Péclet numbers. Nevertheless, little differences appear between these three values of the Péclet number indicating that the velocity is strongly coupled to the thermal behavior. Note that the velocity profiles localized downstream to $L_{\mathrm{iso}-T_g}$ are closer than usual power-law fluid profiles. However, these profiles confirm that the flow is not the simple solution of an iso-thermal power-law model as it has been suspected in [5]. In such material characterized by a large Prandtl number, the ratio of the kinematic viscosity to the thermal diffusivity, the fluid dynamics is the slave of the thermal solution mainly due to the viscosity dependence on temperature.

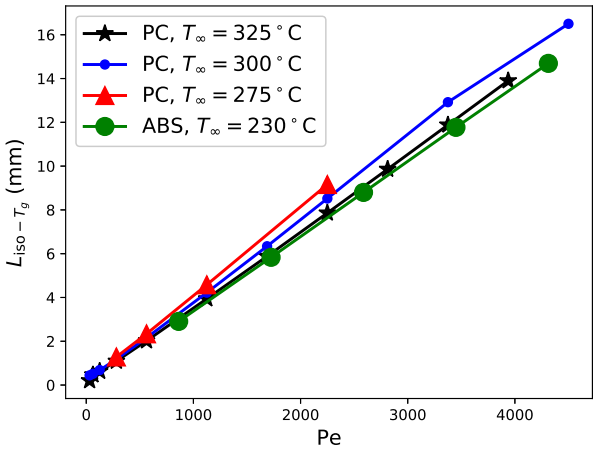

Figure 7: $L_{\mathrm{iso}-T_g}$ (mm) as a function of Pe for the bisphenol-A polycarbonate and the acrylonitrile butadiene styrene.

3.2. Behavior of $L_{\mathrm{iso}-T_g}$ *vs.* Pe

As it has been observed in the previous subsection, the spreading of the domain where the temperature is below the glass transition one increases with the Péclet number. It results in the competition of heat transfer by advection and diffusion studied for a long time [20]. Nevertheless, the quantification of $L_{\mathrm{iso}-T_g}$ as a function of the working conditions of the 3D printer is an important issue. Indeed as reported in the recent work of Mackay et al. [9], above a threshold of inlet velocity, the 3D printer fails to provide an extrudate.

Previously, $L_{\mathrm{iso}-T_g}$ has been reported for three particular Péclet numbers. To go further, numerical simulations have been done for a large range of Péclet numbers. Moreover, two lower temperatures of the liquefier have been investigated equally to 300 to 275°C. Finally, numerical simulations have been performed for an acrylonitrile butadiene styrene which properties are given in Appendix A (the glass transition temperature is equal to 105°C). The inlet temperature stays the same, i.e. $T_{\mathrm{in}} = 24$°C. The liquefier temperature is set equal to 230°C.

Figure 7 provides the behavior of $L_{\mathrm{iso}-T_g}$ as a function of Péclet number for the bisphenol-A polycarbonate at three liquefier temperatures and for the acrylonitrile butadiene styrene with $T_\infty = 230$°C. Whatever the heating condition and the polymer, $L_{\mathrm{iso}-T_g}$ increases linearly with the Péclet number. The result arises directly from the scaling of the Graetz problem with an imposed temperature on the wall. Indeed, according to Bejan [21, sec. 3.5], heat transfer can be written in reduced variables for which the axial characteristic length is proportional to Pe. Even if this scaling is established for a Newtonian fluid, it does not change for a generalized Newtonian fluid. Consequently, it is expected to find a distance to reach the glass transition temperature scaling linearly with the Péclet number.

For the bisphenol-A polycarbonate, the slope of $L_{\mathrm{iso}-T_g}$ as a function of Pe increases with the reduction of the liquefier temperature T_∞. The decrease of T leads to a larger distance to reach T_g in the liquefier for the polymer. To see the effect of the heating,

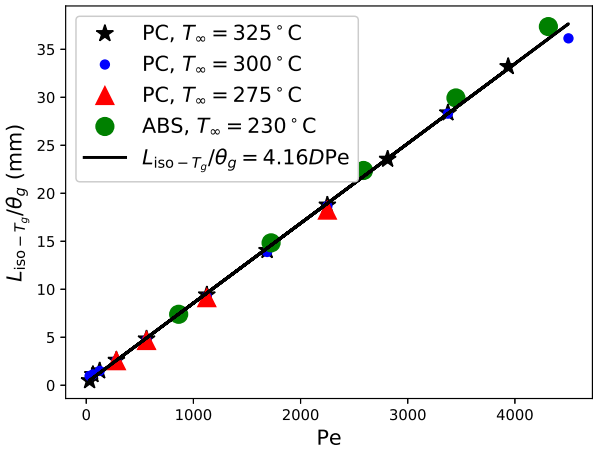

Figure 8: $L_{\mathrm{iso}-T_g}/\theta_g$ (mm) as a function of Pe for the bisphenol-A polycarbonate and the acrylonitrile butadiene styrene.

the inlet temperature and also the nature of the polymer (various T_g), $L_{\mathrm{iso}-T_g}$ divided by $\theta_g = (T_g - T_0)/(T_\infty - T_0)$ is plotted as function of the Péclet number in Figure 8. All data merge in a master curve. A linear fitting gives that $L_{\mathrm{iso}-T_g}$ can be written as follows

$$L_{\mathrm{iso}-T_g} = 4.16 \cdot 10^{-3} \theta_g D\,\mathrm{Pe}\,. \tag{15}$$

This result can be exploited to provide the correct working conditions of the 3D printer liquefier. Indeed, replacing $L_{\mathrm{iso}-T_g}$ by the entire distance of the liquefier L in equation (15) gives the threshold of the Péclet number above which the polymer is not completely heated above T_g. From the definitions of the reduced variables, the limit of the inlet velocity can be written as follows

$$U_{\mathrm{in}} = 2.41 \cdot 10^{2} \frac{T_\infty - T_0}{T_g - T_0} \frac{\lambda}{\rho C_p} \frac{d^2 L}{D^4}. \tag{16}$$

This relation gathers working parameters such as the inlet and heating temperature but also various characteristics of the polymer and geometry of the liquefier.

4. Conclusion

The present work focuses on the numerical computations of the polymer heating in the liquefier of a FFF additive manufacturing printer with a finite element method. The heat and mass transfer equations are solved taking into account the temperature and shear dependence of the dynamic viscosity in the whole temperature range (above and below the glass transition temperature). The geometry is chosen according to the previous contribution of Peng et al. [5]. Only amorphous polymers are considered such as polycarbonate and acrylonitrile butadiene styrene.

The numerical results confirm the previous observations of Peng et al. [5] of a perfect thermal contact between the polymer and the wall of the liquefier. The kinematics is

characterized by the occurrence of a plug flow close to the inlet showing the strong coupling between temperature and velocity fields. The spatial limit of the iso-T_g curve is also investigated showing that the spread of the core with a temperature less than T_g increases linearly with the inlet velocity. A limit in terms of inlet velocity is provided with a simple relation easy to use as a function of polymer properties and geometrical data.

This work has to be completed soon by taking into account the viscoelasticity of the polymer to study more clearly the solid to liquid transition. Moreover, an integrated computation of the polymer behavior in the liquefier and during the spreading process on the substrate is on the way. It will especially allow investigating the influence of the temperature heterogeneity at nozzle exit on the dimensions of the deposited layer.

A. Properties of polycarbonate and acrylonitrile butadiene styrene polymers

A.1. Bisphenol-A PC polymer

According to Peng et al. [5], the bisphenol-A polycarbonate used for experiments is Makrolon® 3208 provided by Covestro. From the viscosity data provided by the supplier at three temperatures [22], the parameters η_0, λ, n, a, E_a have been determined in two steps. First, the shift factors are determined to superimpose the whole data in the plane $(\dot{\gamma}a_T, \eta/a_T)$ by taking the reference temperature equal to 320°C. Using the law given by Eq. (4), the activation energy is then obtained by a linear regression. The correlation coefficient is very close to 1. In the second step, parameters η_0, λ and n are determined by a non-linear regression technique using a routine in Python. According to Hieber and Chiang [13], the parameter a is set equal to one for the bisphenol-A PC polymer. Table 3 summarizes parameters of the Carreau-Yasuda and the Arrhenius laws. The reference temperature is also given in Table 3.

η_0	λ	n	a	E_a	T_{ref}
Pa·s	s	–	–	kJ/mol	K
529.17	$1.19{\cdot}10^{-3}$	0.31	1.	100.9	593.15

Table 3: Parameters of the Carreau-Yasuda and Arrhenius laws for the bisphenol-A polycarbonate (Makrolon® 3208).

Figure 9 depicts η/a_T as a function of $\dot{\gamma}a_T$ according to the data provided in [22]. The solid line corresponds to the Carreau-Yasuda's law fitting with the parameters given in Table 3. The maximum error between the data given by [22] and the Carreau-Yasuda's law is equal to 2.3%

ρ	C_p	k
kg/m^3	J/(kg·K)	W/(m·K)
1200	1250	0.2

Table 4: Density, heat capacity and thermal conductivity of the bisphenol-A polycarbonate (Makrolon® 3208) according to [22] and [23].

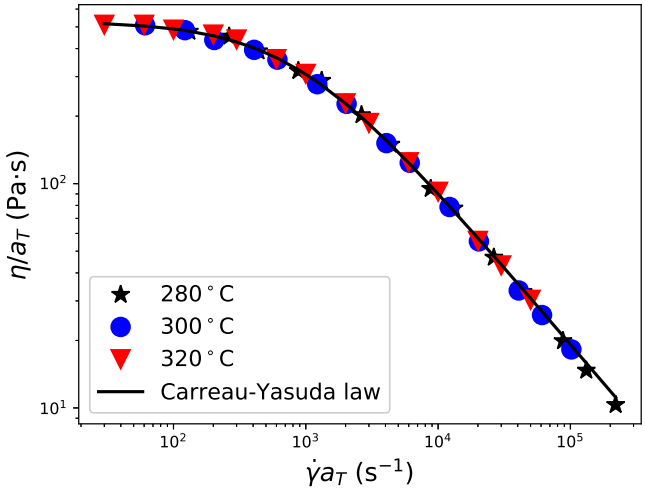

Figure 9: $\eta(\dot{\gamma}, T)/a_T$ vs. $\dot{\gamma}a_T$ for the bisphenol-A polycarbonate (Makrolon® 3208) at three temperatures.

For the bisphenol-A polycarbonate polymer, the density, the thermal conductivity, and the heat capacity are given in Table 4. The values of ρ and k are taken from the datasheet [22] while the heat capacity comes from the handbook of Mark [23].

A.2. ABS polymer

The acrylonitrile butadiene styrene (ABS) has been bought an Internet platform dedicated to 3D printer materials (Grossiste.com). A parallel plate rheometer ARES from TA Instruments is used for the viscosity measurements. The dynamic viscosity has been determined at 210, 220, 230 and 240°C. The same procedure detailed above has been employed for the ABS polymer by setting $a = 0.6$ and $T_{\text{ref}} = 220$°C. Table 5 gives the parameters of the dynamic viscosity defined by (1) and the Arrhenius law, eq. (4).

η_0	λ	n	a	E_a	T_{ref}
Pa·s	s	–	–	kJ/mol	K
$3.04 \cdot 10^3$	$3.2{\cdot}10^{-2}$	0.28	0.6	115.06	493.15

Table 5: Parameters using in the Carreau-Yasuda and Arrhenius laws for the acrylonitrile butadiene styrene.

Figure 10 presents the experimental data of the reduced dynamic viscosity $\eta(\dot{\gamma}, T)/a_T$ as a function of $\dot{\gamma}a_T$. The maximum of the relative error given by the Carreau-Yasuda's law is equal to 4.4%. It is noteworthy that for the ABS polymer the transition between the Newtonian plateau and the power-law regime is wider than for the bisphenol-A PC polymer.

The thermal properties are gathered in Table 6 according to the data provided by Mackay et al. [9]. It is noteworthy to underline that the heat capacity of the acrylonitrile butadiene styrene is two times larger than the heat capacity of the bisphenol-A polycarbonate.

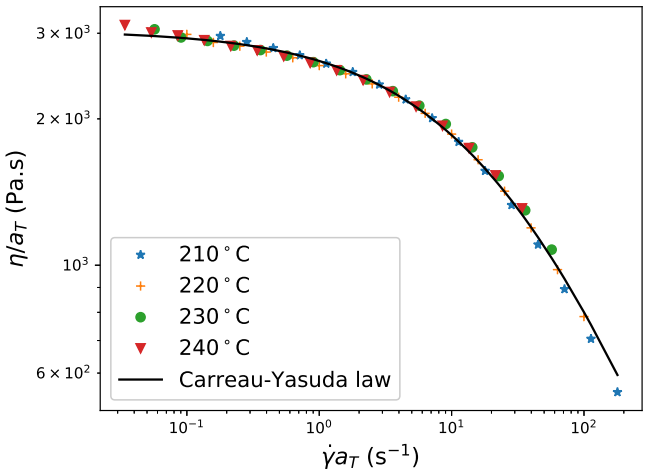

Figure 10: $\eta(\dot{\gamma}, T)/a_T$ vs. $\dot{\gamma}a_T$ for the ABS polymer at four temperatures and solution obtained from the Carreau-Yasuda's law.

ρ	C_p	k
kg/m^3	J/(kg·K)	W/(m·K)
1150	2100	0.21

Table 6: Density, heat capacity and thermal conductivity of the acrylonitrile butadiene styrene according to [9].

References

[1] B. N. Turner, R. Strong, and S. A. Gold. A review of melt extrusion additive manufacturing processes: I. process design and modeling. *Rapid Prototyping J.*, 20(3):192–204, 2014.

[2] H. Bikas, P. Stavropoulos, and G. Chryssolouris. Additive manufacturing methods and modelling approaches: a critical review. *Int. J. Adv. Manuf. Technol.*, 83(1-4):389–405, Jul 2015.

[3] J. M. Lee, S. L. Sing, M. Zhou, and W. Y. Yeong. 3d bioprinting processes: A perspective on classification and terminology. *Int. J. Bioprinting*, 2018.

[4] G. D. Goh, Y. L. Yap, H. K. J. Tan, S. L. Sing, G. L. Goh, and W. Y. Yeong. Process–structure–properties in polymer additive manufacturing via material extrusion: A review. *Crit. Rev. Solid State Mater. Sci.*, 0(0):1–21, 2019.

[5] F. Peng, B. D. Vogt, and M. Cakmak. Complex flow and temperature history during melt extrusion in material extrusion additive manufacturing. *Addit. Manuf.*, 22:197 – 206, 2018.

[6] S. F. Costa, F. M. Duarte, and J.A. Covas. Thermal conditions affecting heat transfer in FDM/FFE: a contribution towards the numerical modelling of the process. *Virtual Phys. Prototy.*, 10(1):35–46, 2015.

[7] A. Bellini, S. Guceri, and M. Bertoldi. Liquefier dynamics in fused deposition. *J. Manuf. Sci. Eng.*, 126(2):237–246, 2004.

[8] G. B. Arfken, H. J. Weber, and F. E. Harris, editors. *Mathematical Methods for Physicists. A Comprehensive Guide*. Academic Press, Oxford, seventh edition, 2013.

[9] M. E. Mackay, Z. R. Swain, C. R. Banbury, D. D. Phan, and D. A. Edwards. The performance of the hot end in a plasticating 3D printer. *J. Rheol.*, 61(2):229–236, 2017.

[10] R. B. Bird, R. C. Armstrong, and O. Hassager. *Dynamics of polymeric liquids: Vol. 1 Fluid mechanics*. Wiley-Interscience, 2nd edition, 1987.

[11] H. Xia, J. Lu, S. Dabiri, and G. Tryggvason. Fully resolved numerical simulations of fused deposition modeling. Part I: Fluid flow. *Rapid Prototyping J.*, 24(2):463–476, 2018.

[12] P. J. Carreau. Rheological equations from molecular network theories. *Trans. Soc. Rheol.*, 16(1):99–127, 1972.
[13] C. A. Hieber and H. H. Chiang. Shear-rate-dependence modeling of polymer melt viscosity. *Polym. Eng. Sci.*, 32(14):931–938, 1992.
[14] R. B. Bird, W. E. Stewart, and E. N. Lightfoot. *Transport phenomena*. John Wiley and sons, New York, second edition, 2002.
[15] M. L Williams, R. F Landel, and J. D Ferry. The temperature dependence of relaxation mechanisms in amorphous polymers and other glass-forming liquids. *J. Am. Chem. Soc.*, 77(14):3701–3707, 1955.
[16] J. R. A. Pearson. Polymer flows dominated by high heat generation and low heat transfer. *Polym. Eng. Sci.*, 18(3):222–229, 1978.
[17] A. Ern and J.-L. Guermond. *Theory and practice of finite elements*, volume 159. Springer Science & Business Media, 2004.
[18] J.-F. Agassant, F. Pigeonneau, L. Sardo, and M. Vincent. Flow analysis of the polymer spreading during extrusion additive manufacturing. *Addit. Manuf.*, 29:100794, 2019.
[19] P. Saramito. *Efficient C++ finite element computing with Rheolef*. CNRS-CCSD ed., version 7.0 edition, 2018.
[20] L. Graetz. Ueber die wärmeleitungsfähigkeit von flüssigkeiten. part 1. *Ann. Phys. Chem.*, 18:79–94, 1883.
[21] A. Bejan. *Convection heat transfer*. John Wiley & Sons, Hoboken, New Jersey, third edition, 2013.
[22] Bayer Material Science. *Makrolon® 3108, 3158 and 3208*, 2008.
[23] J. E. Mark, editor. *Physical properties of polymers handbook*. Springer, second edition, 2007.